Thermography process and topological asymptotic formula for tumor detection

Emna Ghezaiel, Maatoug Hassine

Thermography process and topological asymptotic formula for tumor detection

Emna GHEZAIEL[1] **and Maatoug HASSINE**[2]

[1]ESSTHS, Sousse University, Tunisia
[2]FSM, Monastir University, Tunisia

*E-mail : E-mail : ghezaiel.emna@gmail.com, maatoug.hassine@enit.rnu.tn

Abstract

This work is concerned with a geometric inverse problem related to the thermography concept. The aim is the identification of the shape, size and location of a small embedded tumor from measured temperature on the skin surface. The temperature distribution in the biological tissue is governed by the Pennes model equation. Our proposed approach is based on the Kohn-Vogelius formulation and the topological sensitivity analysis method. The ill-posed geometric inverse problem is reformulated as a topology optimization one. The topological gradient is exploited for locating the zone containing the embedded tumor. The size and shape of the infected zone are approximated using the solution of a scalar parameter estimate problem. The efficiency and accuracy of the proposed approach are justified by some numerical simulations.

Keywords

Bio-heat transfer; tumor reconstruction; Kohn-Vogelius formulation; topological sensitivity analysis; parabolic operator; topology optimization; numerical simulation

I INTRODUCTION

Due to the advanced technology development, thermography or infrared thermal imaging has become a very valuable tool in medicine for various applications like blood perfusion monitoring, breast cancer diagnostics, fever screening, dermatological applications, dental diagnostics, therapeutic assessment, diagnosis of vascular disorder, eye disease, as well as for diagnosis of thyroid gland disease [21, 20, 13, 6, 18]. It provides a non-invasive diagnostic method based on the bioheat transfer of the observed tissue. The infrared cameras (IR) are used to detect and measure the thermal radiation that is being emitted from the skin's surface. In this process the temperature can be evaluated based on the intensity and emissivity of the examined surface. Thermography for diagnostics or medical diagnosis can be carried out using two basic ways: the first one is known as static (or passive) approach. It involves recording the temperature of the observed skin surface under steady-state conditions, which take a lot of time since the patient has to adapt to the environment in the temperature controlled room [1]. The second one is known as dynamic (or active) approach. It consists in creating thermal stress by cooling or heating the investigated tissue followed by quantifying the thermal response during the testing phase, which does not require patient acclimatization and can provide more information about the skin under examination [13, 18]. It has been reported by many research studies that the dynamic infrared thermography has an important advantage over the static one and can besuc-

cessfully used in dermatology for early skin tumor detection [13, 6, 18]. Indeed, skin lesion has higher metabolic heat generation and blood perfusion rate [7] than the healthy skin, which reflected in temperature variations that can be recorded using IR cameras. For an early stage tumor, the temperature difference between lesion and healthy skin is very small in such away it cannot be detected using the static thermography. This difficulty is overcome by the dynamic thermography due to the created thermal stresses by cooling the investigated tissue. Such an approach allows to have higher temperature contrast during the diagnostic process that can be easily observed [12]. Thereby, the recorded temperature measurements can be exploited to identify several tumor parameters (like position, size, blood perfusion rate, ... etc) by means of solving an inverse problem. In this study, we use the dynamic thermography as a medical diagnostic tool and we develop a fast and efficient detection procedure for identifying location and size of skin tumors from surface temperature measurements. This study is motivated by the fact that early detection of cancer increases the patient's chances of survival tremendously. For instance, if the melanoma (fatal cancer) is detected and treated early the survival rate is about 98 %, however the survival rate of patient drops sharply to 15% when the tumor has penetrated into the epidermis layer [9].

1.1 Mathematical model equations

Different skin models have been developed and numerically implemented by mathematicians, physicists and biologists for solving a variety of applications such as; evaluating the efficacy of cancer drugs, detecting tumors in early stages, simulating the inflammation in an injured tissue, ... etc. In the more realistic models, that have been tested in clinical trials, the skin tissue have been modeled by multiple layers of different thermophysical properties: epidermis, papillary dermis, reticular dermis, fat layer, muscle layer (See figure 1).

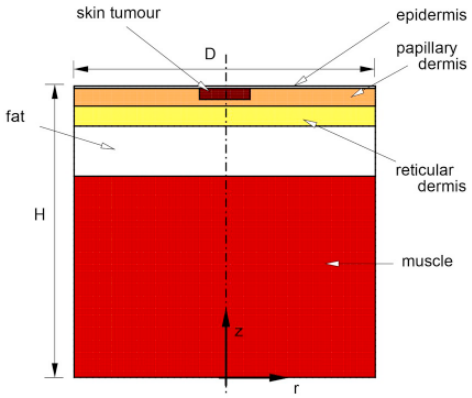

Figure 1: Layers of skin tissue [12].

In this section, we present the mathematical model equations that have been used in the implementation of the dynamic thermography process. The most used models are based on two main aspects. The first one concerns the heat transfer process in a biological tissue. The second aspect concerns the local thermoregulation response of the examined tissue.

• *Bioheat transfer model :* The most important aspects of this model are taken from Çetingűl and Herman [7]. The Pennes equation [17] has been used for describing the bioheat transfer process

$$\rho c_p \frac{\partial \mathcal{T}}{\partial t} - \operatorname{div}(\sigma \nabla \mathcal{T}) - \varpi_b \rho_b c_b (\hbar_a - \mathcal{T}) = \mathcal{S}, \tag{1}$$

where $\mathcal{T}$ represents the temperature distribution in the considered tissue, ρ is the effective tissue density, σ is the thermal conductivity, c_p is the specific heat, ϖ_b is the blood perfusion coeffi-

cient, ρ_b is the density of the blood, c_b the specific heat of the blood, $\hbar_a$ is the artery temperature and $\mathcal{S}$ is the metabolic heat source.

In this model equation, it is assumed that the heat transfer between the blood flow and the surrounding tissue occurs on the capillary level owing to the large interfacial area. Therefore, the blood perfusion term plays the role of heat source or sink depending on the difference of the temperature between arterial blood flow and tissue. During the cooling step of the dynamic thermography, the blood perfusion acts as a heat source term heating up the tissue during the thermal recovery similarly to the metabolic heat source. Here, it is important to note that the tissue properties and other parameters in the previous Pennes equation are usually considered as constants, because there is no accurate mathematical models for describing theirs behaviors.

• *Thermoregulation model :* It is concluded in many studies that blood perfusion rate and metabolic heat generation of skin are controlled by central and local thermoregulation [19, 10]. Therefore, to improve the accuracy of the bioheat transfer model during the cooling-rewarming process of the dynamic thermography, the local thermoregulation response of the tissue needs to be taken into account in the model. The basic concept of the proposed model has been taken from Silva et al [19] and Fiala et al [10], where the local tissue temperature response has been modeled with the help of an exponential temperature distribution when simulating the thermoregulation of whole body.

- The metabolic heat generation has been modeled using the Van't Hoff effect [19, 10];

$$\mathcal{S}(\mathcal{T}) = q_{m,bas}\, Q_{10,m}^{\left(\frac{\mathcal{T}-\mathcal{T}_0}{10}\right)} \tag{2}$$

  with $q_{m,bas}$ denotes the basal metabolic rate at rest, $Q_{10,m}$ is the metabolic rate coefficient and $\mathcal{T}_0$ is the equilibrium temperature of the body.
- Since the blood perfusion rate is in correlation with the metabolic rate by oxygen and nutrition demand, the blood perfusion rate in skin tissue has been usually modeled similarly to the heat generation as

$$\varpi_b(\mathcal{T}) = \varpi_{b,bas}\, Q_{10,b}^{\left(\frac{\mathcal{T}-\mathcal{T}_0}{10}\right)} \tag{3}$$

  with $\varpi_{b,bas}$ denotes the basal blood perfusion rate and $Q_{10,b}$ is the blood perfusion rate coefficient, which is usually equal to $Q_{10,m}$ [19].

1.2 Research studies

In recent years, new techniques for tumors diagnostic have been developed involving a compromise between specific aspects (like accuracy, effectiveness, cost) and invasiveness like ultrasound and magnetic resonance imaging (MRI), multispectral imaging systems, digital photography, confocal scanning laser microscopy (CSLM), laser Doppler perfusion imaging (LDPI) optical coherence tomography(OCT) [16]. Due to the technology development many research studies have been conducted focusing on various issues related to the tumors detection problems such as the bioheat transfer modeling, estimation of skin tumors parameters, early tumors detection, dynamic thermography process, modeling of laser treatment [15, 14].

In the context of tumors detection, Cheng and Herman [8] proposed a simple 2D numerical model for skin tumor identification based on the dynamic thermography process. They employed multiple tissue layers and presented different skin cooling approaches for dynamic thermography. Therefore, they numerically solved several direct bioheat problems for recovering which properties (cooling time, heat transfer coefficients, cooling temperature) have the greatest influence on the temperature difference between the lesion and the surrounding tissue. Çeting˝ul and Herman [7] used 3D skin model taking into account the presence of different tissue

layers (epidermis, muscle, reticular dermis, fat, papillary dermis and lesion) for describing the rewarming process of dynamic thermography. In [7], they numerically examined how the esion shape affects the distribution of temperature on the skin surface as well as the influence of some model parameters such as thickness, blood perfusion rate and thermal conductivity.

Similar numerical approaches have been investigated by Bhowmik et al [4, 5] for estimating the thickness, diameter, metabolic heat generation and blood perfusion rate of the skin tumor using static thermography. The presented works in [4, 5] are concerned with tumor identification in its early stage. In [4], the lesion identification process is affected by the included thermally significant vessels in the skin model. This identification approach has been improved in [5] using Frequency Modulated Thermal Wave Imaging (FMTWI).

1.3 Proposed approach

In this work, we deal with a geometric inverse problem related to the thermography concept. We develop a fast and accurate approach for identifying the shape, size and location of a small embedded tumor from over-determined boundary data (an imposed heat flux and a measured temperature) at the skin surface. Our main tool is based on the the Kohn-Vogelius formulation [2] and the topological sensitivity analysis method [11, 3].

In this work, we extend this approach for solving a biological inverse problem. In this context, the sensitivity analysis method leads to derive a topological asymptotic expansion for the Pennes equation with respect to the presence of a small tumor inside the examined skin tissue. Actually, the tumor should be modeled by an inclusion with different material properties from the background embedded within the healthy tissue. But in this configuration, the mathematical analysis becomes further complicated, since all coefficients of the Pennes equation would be subject to topological perturbations. For these reasons, we limit ourselves to a simplified model based on the following assumptions :

∘ The embedded tumor is modeled as a sub-region where the temperature reaches its maximum.

∘ The temperature distribution in the biological tissue is governed by the linear Pennes equation.

In this study, according to the Kohn-Vogelius concept the ill-posed geometric inverse problem (in Hadamard's sense) is reformulated as a topology optimization one. The over-determined boundary data (Neumann and Dirichlet conditions) are exploited for defining two well-posed auxiliary parabolic systems. The misfit function to be minimized is constructed using the screpancy between the auxiliary problems solutions. The topological gradient is used for locating the zone containing the embedded tumor. The size and shape of the infected zone are approximated using the solution of a scalar parameter estimate problem. The efficiency and accuracy of the proposed approach are justified by some numerical simulations.

II INVERSE PROBLEM

Let $\Omega \subset \mathbb{R}^2$ be a smooth and bounded domain represents the considered biological tissue. Let $\mathcal{I}^*$ be an unknown tumor embedded inside the tissue Ω. It is modeled as an infected small sub-region that are characterized by a maximum temperature peak ($\mathcal{T} \approx \theta_m$ in $\mathcal{I}^*$).

In order to simplify the presentation, we plot in figure 2 a schematic diagram showing an unhealthy tissue Ω containing an infected zone (an embedded tumor) $\mathcal{I}^*$ and the different components of the boundary $\partial\Omega$.

In this configuration example, the temperature field satisfies a non flux condition $\sigma \nabla \mathcal{T} . \eta = 0$ on the lateral boundaries Γ_l. On the bottom boundary Γ_b, a constant core temperature θ_c is

prescribed. Aiming to detect the unknown anomaly zone $\mathcal{I}^*$, we will use over-determined boundary data given on the outer surface Σ_s of the tissue (skin surface).

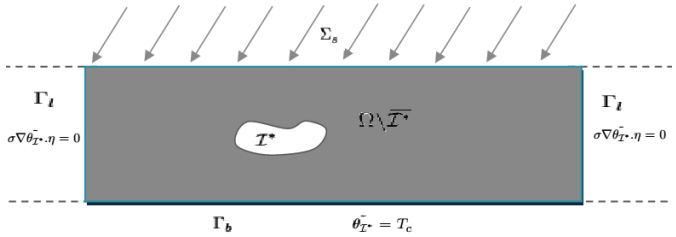

Figure 2: Schematic diagram: an infected tissue Ω containing an embedded tumor $\mathcal{I}^*$.

The geometric inverse problem that we consider can be formulated as follows:

- Knowing two boundary data on the accessible surface Σ_s: an imposed heat flux θ_n (a Neumann condition) and a measured temperature θ_d (a Dirichlet condition)
- Determine the location, size and shape of the unknown embedded tumor $\mathcal{I}^*$, in such a way that the temperature distribution $\mathcal{T}^*$ in the unhealthy tissue satisfies the following bio-heat transfer system

$$\left\{\begin{array}{rcll} \rho c_p \dfrac{\partial \mathcal{T}^*}{\partial t} - \text{div}\,(\sigma\nabla\mathcal{T}^*) - \varpi_b\rho_b c_b(\hbar_a - \mathcal{T}^*) &= \mathcal{S} & \text{in} & \Omega\backslash\overline{\mathcal{I}^*}\times]0,T[, \\ \mathcal{T}^* &= \theta_c & \text{on} & \Gamma_b\times]0,T[, \\ \sigma\nabla\mathcal{T}^*.\eta &= 0 & \text{on} & \Gamma_l\times]0,T[, \\ \mathcal{T}^* &= \theta_m & \text{on} & \partial\mathcal{I}^*\times]0,T[, \\ \mathcal{T}^*(.,0) &= \theta_0 & \text{in} & \Omega\backslash\overline{\mathcal{I}^*}. \end{array}\right. \tag{4}$$

with an over-specified boundary condition on the skin surface

$$\begin{array}{rcll} \sigma\nabla\mathcal{T}^*.\eta &= \theta_n & \text{on} & \Sigma_s\times]0,T[, \\ \mathcal{T}^* &= \theta_d & \text{on} & \Sigma_s\times]0,T[. \end{array} \tag{5}$$

In (4), θ_0 denotes the temperature distribution in the tissue.

To analyze this geometric inverse problem, we will develop an efficient approach based on the Kohn-Vogelius method and the topological sensitivity concept.

III TOPOLOGY OPTIMIZATION PROBLEM

We begin by reformulating the previous inverse problem as a topology optimization one. Using the Kohn-Vogelius formulation, for each admissible anomaly zone, we introduce two auxiliary problems. The first one is defined using the imposed heat flux on the boundary Σ_s

$$\left\{\begin{array}{rcll} \rho c_p \dfrac{\partial \mathcal{T}^N}{\partial t} - \text{div}\,(\sigma\nabla\mathcal{T}^N) - \varpi_b\rho_b c_b(\hbar_a - \mathcal{T}^N) &= \mathcal{S} & \text{in} & \Omega\backslash\overline{\mathcal{I}}\times]0,T[, \\ \sigma\nabla\mathcal{T}^N.\eta &= \theta_n & \text{on} & \Sigma_s\times]0,T[, \\ \mathcal{T}^N &= \theta_c & \text{on} & \Gamma_b\times]0,T[, \\ \sigma\nabla\mathcal{T}^N.\eta &= 0 & \text{on} & \Gamma_l\times]0,T[, \\ \mathcal{T}^N &= \theta_m & \text{on} & \partial\mathcal{I}\times]0,T[, \\ \mathcal{T}^N(.,0) &= \theta_0 & \text{in} & \Omega\backslash\overline{\mathcal{I}}. \end{array}\right. \tag{6}$$

The second one is called "Dirichlet problem" deefined using the measured temperature on Σ_s

$$\left\{\begin{array}{rcll} \rho c_p \dfrac{\partial \mathcal{T}^D}{\partial t} - \text{div}\,(\sigma \nabla \mathcal{T}^D) - \varpi_b \rho_b c_b (\hbar_a - \mathcal{T}^D) & = \mathcal{S} & \text{in} & \Omega\backslash\overline{\mathcal{I}}\times]0,T[, \\ \mathcal{T}^D & = \theta_d & \text{on} & \Sigma_s\times]0,T[, \\ \mathcal{T}^D & = \theta_c & \text{on} & \Gamma_b\times]0,T[, \\ \sigma\nabla\mathcal{T}^D.\eta & = 0 & \text{on} & \Gamma_l\times]0,T[, \\ \mathcal{T}^D & = \theta_m & \text{on} & \partial\mathcal{I}\times]0,T[, \\ \mathcal{T}^D(.,0) & = \theta_0 & \text{in} & \Omega\backslash\overline{\mathcal{I}}. \end{array}\right. \tag{7}$$

One can remark here that if $\mathcal{I}$ coincides with the actual infected zone $\mathcal{I}^*$, then the misfit between the Neumann and Dirichlet solutions vanishes. Starting from this observation, we propose an identification process based on the minimization of the following Kohn-Vogelius type functional

$$\mathcal{F}(\Omega\backslash\overline{\mathcal{I}}) = \int_0^T \int_{\Omega\backslash\overline{\mathcal{I}}} |\mathcal{T}^N(\mathcal{I}) - \mathcal{T}^D(\mathcal{I})|^2 dxdt,$$

where $\mathcal{T}^N(\mathcal{I})$ and $\mathcal{T}^D(\mathcal{I})$ are the solutions, respectively, to (6) and (7).

Then, the considered geometric inverse problem can be reformulated as a topology optimization one where the unknown infected zone $\mathcal{I}^*$ is characterized as the solution to

$$(\mathcal{P}_{min}) \left\{ \begin{array}{l} \text{Find the location, size and shape of the domain } \mathcal{I}^* \text{ such that} \\ \mathcal{F}(\Omega\backslash\overline{\mathcal{I}^*}) = \min\limits_{\mathcal{I}\in\mathcal{D}_{ad}} \mathcal{F}(\Omega\backslash\overline{\mathcal{I}}), \end{array}\right.$$

where $\mathcal{D}_{ad}$ is a set of admissible domains $\mathcal{D}_{ad} = \left\{\mathcal{I} \subset \Omega;\ \text{ such that } \partial\mathcal{I} \text{ of class } \mathcal{C}^1 \text{ and } \overline{\mathcal{I}} \subset \Omega\right\}$.
To solve this optimization problem, we shall use the topological sensitivity analysis method.

3.1 Topological sensitivity analysis

The topological sensitivity analysis method consists in studying the variation of the function to be minimized with respect to the creation of a small geometric perturbation inside the domain Ω. The adaptation of this technique to our problem leads to evaluate the Kohn-Vogelius functional variation with respect to the presence of a small infected zone inside the tissue Ω.

Let $\mathcal{I}_{z,\varepsilon} = z + \varepsilon\mathcal{I}$ be a small infected zone, located around an arbitrary point $z \in \Omega$. Its size is described by a small parameter $\varepsilon > 0$, such that $\overline{\mathcal{I}_{z,\varepsilon}}$ is strictly included in Ω. The shape of the anomaly $\mathcal{I}_{z,\varepsilon}$ is given by a given bounded and smooth domain $\mathcal{I} \subset \mathbb{R}^2$ containing the origin.

Practically, this approach requires the development of an asymptotic expansion of the form

$$\mathcal{F}(\Omega\backslash\overline{\mathcal{I}_{z,\varepsilon}}) = \mathcal{F}(\Omega) + \phi(\varepsilon)\mathcal{G}(z) + o\big(\phi(\varepsilon)\big), \text{ where}$$

- $\mathcal{G} : \Omega \longmapsto \mathbb{R}$ is a scalar function (called the topological gradient of $\mathcal{F}$), represents the leading term of the variation $\mathcal{F}(\Omega\backslash\overline{\mathcal{I}_{z,\varepsilon}}) - \mathcal{F}(\Omega)$ with respect to the insertion of a small hole inside the domain Ω.
- $\phi : \mathbb{R}_+ \longmapsto \mathbb{R}_+$ is a scalar positive function, represents the asymptotic behavior of the variation $\mathcal{F}(\Omega\backslash\overline{\mathcal{I}_{z,\varepsilon}}) - \mathcal{F}(\Omega)$ with respect to the geometric perturbation size ε.

IV TOPOLOGICAL ASYMPTOTIC FORMULA

This section is concerned with the development of an asymptotic formula describing the variation of the function

$$\mathcal{F}(\Omega\backslash\overline{\mathcal{I}_{z,\varepsilon}}) = \int_0^T \int_{\Omega\backslash\overline{\mathcal{I}_{z,\varepsilon}}} |\mathcal{T}_\varepsilon^N - \mathcal{T}_\varepsilon^D|^2 dxdt,$$

$\mathcal{F}$ with respect to the presence of a small anomaly $\mathcal{I}_{z,\varepsilon}$ inside the tissue Ω. Here $\mathcal{T}_\varepsilon^N$ and $\mathcal{T}_\varepsilon^D$ are the solutions to the following systems

$$\left\{\begin{array}{rlll} \rho c_p \dfrac{\partial \mathcal{T}_\varepsilon^N}{\partial t} - \text{div}\,(\sigma\nabla\mathcal{T}_\varepsilon^N) + \varpi_b\rho_b c_b \mathcal{T}_\varepsilon^N = \Re & \text{in} & \Omega\backslash\overline{\mathcal{I}_{z,\varepsilon}}\times]0,T[, \\ \sigma\nabla\mathcal{T}_\varepsilon^N.\eta = \theta_n & \text{on} & \Sigma_s\times]0,T[, \\ \mathcal{T}_\varepsilon^N = \theta_c - \theta_m & \text{on} & \Gamma_b\times]0,T[, \\ \sigma\nabla\mathcal{T}_\varepsilon^N.\eta = 0 & \text{on} & \Gamma_l\times]0,T[, \\ \mathcal{T}_\varepsilon^N = 0 & \text{on} & \partial\mathcal{I}_{z,\varepsilon}\times]0,T[, \\ \mathcal{T}_\varepsilon^N(.,0) = \theta_0 - \theta_m & \text{in} & \Omega\backslash\overline{\mathcal{I}_{z,\varepsilon}}. \end{array}\right. \tag{8}$$

$$\left\{\begin{array}{rlll} \rho c_p \dfrac{\partial \mathcal{T}_\varepsilon^D}{\partial t} - \text{div}\,(\sigma\nabla\mathcal{T}_\varepsilon^D) + \varpi_b\rho_b c_b \mathcal{T}_\varepsilon^D = \Re & \text{in} & \Omega\backslash\overline{\mathcal{I}_{z,\varepsilon}}\times]0,T[, \\ \mathcal{T}_\varepsilon^D = \theta_d - \theta_m & \text{on} & \Sigma_s\times]0,T[, \\ \mathcal{T}_\varepsilon^D = \theta_c - \theta_m & \text{on} & \Gamma_b\times]0,T[, \\ \sigma\nabla\mathcal{T}_\varepsilon^D.\eta = 0 & \text{on} & \Gamma_l\times]0,T[, \\ \mathcal{T}_\varepsilon^D = 0 & \text{on} & \partial\mathcal{I}_{z,\varepsilon}\times]0,T[, \\ \mathcal{T}_\varepsilon^D(.,0) = \theta_0 - \theta_m & \text{in} & \Omega\backslash\overline{\mathcal{I}_{z,\varepsilon}}. \end{array}\right. \tag{9}$$

with $\Re = \mathcal{S} + \varpi_b\rho_b c_b(\hbar_a + \theta_m)$. The following theorem summarizes the obtained result.

Theorem IV.1:
The variation of the function $\mathcal{F}$, with respect to the presence of a small internal anomaly $\mathcal{I}_{z,\varepsilon} = z + \varepsilon\mathcal{I}$ inside the tissue domain Ω, satisfies

$$\mathcal{F}(\Omega\backslash\overline{\mathcal{I}}_{z,\varepsilon}) - \mathcal{F}(\Omega) = -\frac{1}{\log\varepsilon}\mathcal{G}(z) + o\big(\frac{-1}{|\log\varepsilon|}\big),$$

where $\mathcal{G}$ is the topological gradient, defined as

$$\mathcal{G}(x) = 2\pi\int_0^T \Big[T_0^N(z,t)\Psi_0^N(z,t) + T_0^D(z,t)\Psi_0^D(z,t)\Big]dt, \forall x\in\Omega,$$

where Ψ_0^N and Ψ_0^D are the solutions to the following auxiliary problems :

$$(A^N)\left\{\begin{array}{rlll} -\rho c_p \dfrac{\partial \Psi_0^N}{\partial t} - \text{div}\,(\sigma\nabla\Psi_0^N) + \varpi_b\rho_b c_b\Psi_0^N = -2(\mathcal{T}_0^N - \mathcal{T}_0^D) & \text{in} & \Omega\times]0,T[, \\ \sigma\nabla\Psi_0^N.\eta = 0 & \text{on} & \Sigma_s\times]0,T[, \\ \Psi_0^N = 0 & \text{on} & \Gamma_b\times]0,T[, \\ \sigma\nabla\Psi_0^N.\eta = 0 & \text{on} & \Gamma_l\times]0,T[, \\ \Psi_0^N(.,T) = 0 & \text{in} & \Omega, \end{array}\right.$$

$$(A^D)\left\{\begin{array}{rlll} -\rho c_p \dfrac{\partial \Psi_0^D}{\partial t} - \text{div}\,(\sigma\nabla\Psi_0^D) + \varpi_b\rho_b c_b\Psi_0^D = -2(\mathcal{T}_0^D - \mathcal{T}_0^N) & \text{in} & \Omega\times]0,T[, \\ \Psi_0^D = 0 & \text{on} & \Sigma_s\times]0,T[, \\ \Psi_0^D = 0 & \text{on} & \Gamma_b\times]0,T[, \\ \sigma\nabla\Psi_0^D.\eta = 0 & \text{on} & \Gamma_l\times]0,T[, \\ \Psi_0^D(.,T) = 0 & \text{in} & \Omega, \end{array}\right.$$

V NUMERICAL EXPERIMENTS

In this section, we propose a fast and efficient numerical procedure for reconstructing the unknown anomalies from over-determined boundary data. The developed algorithm is based on the asymptotic formula presented in Theorem IV.1. The topological gradient $\mathcal{G}$ is exploited for detecting the location, size and shape of the anomalies.
For each $\xi \in [0,1]$, we denote by $\mathcal{I}_\xi := \{x \in \Omega,\ \mathcal{G}(x) \leq \xi \delta_{min}\}$, where δ_{min} the most negative value of the sensitivity function $\mathcal{G}$ in the domain Ω.

Algorithm : one iteration reconstruction procedure

- Solve the direct Neumann and Dirichlet problems.
- Solve the adjoint Neumann and Dirichlet problems.
- Compute the topological gradient $G(z)$, $z \in \Omega$.
- Find $\xi^* \in [0,\ 1]$ such that $\mathcal{F}(\Omega \backslash \overline{\mathcal{I}_{\xi^*}}) \leq \mathcal{F}(\Omega \backslash \overline{\mathcal{I}_\xi}), \forall \xi \in [0,1]$.

Next, we apply our numerical algorithm for identifying two anomalies from noisy boundary measurements data. We denote by δ the level of the noise. We start by an exact boundary measurement (i.e. δ = 0%). In this case, as one can observe in Figure 3(a), the topological gradient detect perfectly the two anomalies (via two strictly negative minima (red zones)).

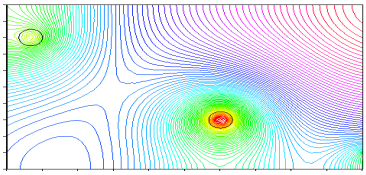

(a) Identification result from exact measured data, i.e. $\delta = 0\%$.

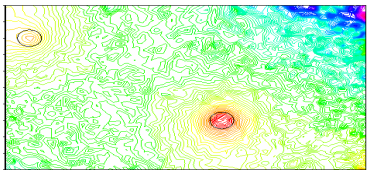

(b) Identification result from noisy measured data, when $\delta = 10\%$.

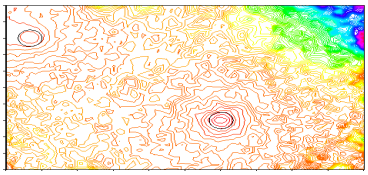

(c) Identification result from noisy measured data, when $\delta = 15\%$.

Figure 3: Effect of the noise on the reconstruction.

From the numerical simulations, we deduce the following remarks:

- When the noise level δ is less than 10% (see figures 3(a) and 3(b)), the topological gradient has two local negative minima, which provides a good detection result for the two unknown anomalies.
- When the noise level is greater that 10% (see figure 3(c)), the amplitude of oscillations in the topological gradient values becomes large in such a way the actual anomalies cannot be detected.

REFERENCES

[1] K. Ammer and E. Ring. Standard procedures for infrared imaging in medicine. *Biomedical Engineering Handbook, CRC Press*, 1, 2006.

[2] S. Andrieux, T. Baranger, and A. Benabda. Solving cauchy problems by minimizing an energy-like functional. *Inverse problems*, 22(1):115, 2006.

[3] A. Benabda, M. Hassine, M. Jaoua, and M. Masmoudi. Topological sensitivity analysis for the location of small cavities in stokes flow. *SIAM Journal on Control and Optimization*, 48(5):2871–2900, 2009.

[4] A. Bhowmik, R. Repaka, and S. C. Mishra. Thermographic evaluation of early melanoma within the vascularized skin using combined non-newtonian blood flow and bioheat models. *Computers in Biology and Medicine*, 53:206–219, 2014.

[5] A. Bhowmik, R. Repaka, R. Mulaveesala, and S. C. Mishra. Suitability of frequency modulated thermal wave imaging for skin cancer detection—a theoretical prediction. *Journal of thermal biology*, 51:65–82, 2015.

[6] M. Bonmarin and F.-A. Le Gal. Lock-in thermal imaging for the early-stage detection of cutaneous melanoma: a feasibility study. *Comp. biol. med.*, 47:36–43, 2014.

[7] M. P. Çetingül and C. Herman. A heat transfer model of skin tissue for the detection of lesions: sensitivity analysis. *Physics in Medicine & Biology*, 55(19):5933, 2010.

[8] T.-Y. Cheng and C. Herman. Analysis of skin cooling for quantitative dynamic infrared imaging of near-surface lesions. *journal of thermal sciences*, 86:175–188, 2014.

[9] D. Elder. Tumor progression, early diagnosis and prognosis of melanoma. *Acta oncologica*, 38(5):535–548, 1999.

[10] D. Fiala, G. Havenith, P. Bröde, B. Kampmann, and G. Jendritzky. Utci-fiala multi-node model of human heat transfer and temperature regulation. *International journal of biometeorology*, 56(3):429–441, 2012.

[11] M. Hassine and M. Masmoudi. The topological asymptotic expansion for the quasi-stokes problem. *ESAIM: Control, Optimisation and Calculus of Variations*, 10(4):478–504, 2004.

[12] J. Iljaž, L. C. Wrobel, M. Hriberšek, and J. Marn. Numerical modelling of skin tumour tissue with temperature-dependent properties for dynamic thermography. *Computers in Biology and Medicine*, 112:103367, 2019.

[13] B. B. Lahiri, S. Bagavathiappan, T. Jayakumar, and J. Philip. Medical applications of infrared thermography: a review. *Infrared Physics & Technology*, 55(4):221–235, 2012.

[14] J. M. Luna, A. Hernández Guerrero, R. Romero Méndez, and J. L. Luviano Ortiz. Solution of the inverse bio-heat transfer problem for a simplified dermatological application: case of skin cancer. *Ingeniería mecánica, tecnología y desarrollo*, 4(6):219–228, 2014.

[15] P. Partridge and L. Wrobel. An inverse geometry problem for the localisation of skin tumours by thermal analysis. *Eng. Anal. Bound. Elem.*, 31(10):803–811, 2007.

[16] J. K. Patel, S. Konda, O. A. Perez, S. Amini, G. Elgart, and B. Berman. Newer technologies/techniques and tools in the diagnosis of melanoma. *European Journal of Dermatology*, 18(6):617–631, 2008.

[17] H. H. Pennes. Analysis of tissue and arterial blood temperatures in the resting human forearm. *Journal of applied physiology*, 1(2):93–122, 1948.

[18] G. Shi, F. Han, C. Liang, L. Wang, and K. Li. A novel method of thermal tomography tumor diagnosis and its clinical practice. *App. Ther. Eng.*, 73(1):408–415, 2014.

[19] A. B. C. Silva, J. Laszczyk, L. C. Wrobel, F. L. Ribeiro, and A. J. Nowak. A thermoregulation model for hypothermic treatment of neonates. *Medical Engineering & Physics*, 38(9):988–998, 2016.

[20] J.-H. Tan, E. Ng, U. R. Acharya, and C. Chee. Infrared thermography on ocular surface temperature: a review. *Infrared physics & technology*, 52(4):97–108, 2009.

[21] H. Wang, D. R. Wade Jr, and J. Kam. Ir imaging of blood circulation of patients with vascular disease. pages 115–123, 2004.